Voltage-dependent Gating of *Shaker* A-Type Potassium Channels in *Drosophila* Muscle

WILLIAM N. ZAGOTTA and RICHARD W. ALDRICH

From the Department of Neurobiology, Stanford University School of Medicine, Stanford, California 94305

ABSTRACT The voltage-dependent gating mechanism of A_1-type potassium channels coded for by the *Shaker* locus of *Drosophila* was studied using macroscopic and single-channel recording techniques on embryonic myotubes in primary culture. From a kinetic analysis of data from single A_1 channels, we have concluded that all of the molecular transitions after first opening, including the inactivation transition, are voltage independent and therefore not associated with charge movement through the membrane. In contrast, at least some of the activation transitions leading to first opening are considerably voltage dependent and account for all of the voltage dependence seen in the macroscopic currents. This mechanism is similar in many ways to that of vertebrate neuronal voltage-sensitive sodium channels, and together with the sequence similarities in the S4 region suggests a conserved mechanism for voltage-dependent gating among channels with different selectivities. By testing independent and coupled models for activation and inactivation we have determined that the final opening transition and inactivation are not likely to arise from the independent action of multiple subunits, each with simple gating transitions, but rather come about through their aggregate properties. A partially coupled model accurately reproduces all of the single-channel and macroscopic data. This model will provide a framework on which to organize and understand alterations in gating that occur in *Shaker* variants and mutants.

INTRODUCTION

A-type potassium channels in *Drosophila* muscle are coded at least in part by the *Shaker* gene. Mutations in the gene alter transmission at larval neuromuscular junctions (Jan et al., 1977) and eliminate, reduce, or alter A-type currents in embryonic, larval, and adult muscle (Salkoff and Wyman, 1981b; Wu et al., 1983; Zagotta et al., 1988). This A channel has been called A_1 to distinguish it from a second A-type channel found in *Drosophila* neurons, called A_2, which differs in single-channel conductance, voltage dependence, kinetics, and is unaffected by mutations of the *Shaker* locus (Solc et al., 1987; Solc and Aldrich, 1988). Molecular cloning of the *Shaker* gene (Baumann et al., 1987; Kamb et al., 1987; Papazian et al., 1987; Tempel et al.,

Address reprint requests to Dr. Richard W. Aldrich, Department of Neurobiology, Stanford University School of Medicine, Stanford, CA 94305-5401.

J. GEN. PHYSIOL. © The Rockefeller University Press · 0022-1295/90/01/0029/32 $2.00
Volume 95 January 1990 29–60

1987) has revealed similarity in the derived amino acid sequence with other voltage-gated channels that have been cloned; sodium channels from eel electric organ (Noda et al., 1984), rat brain (Noda et al., 1986; Kayano et al., 1988), and *Drosophila* (Salkoff et al., 1987), and calcium channels from vertebrate skeletal muscle (Ellis et al., 1988; Tanabe et al., 1987, 1988).

The homology with the sodium and calcium channels is most extensive in a region that has been called S4 (Noda et al., 1984). This region has a highly conserved recurring motif of a positively charged amino acid at every third position with intervening hydrophobic residues. Present models for voltage-dependent gating favor a mechanism involving a rotation or translation of S4 helices through the membrane. In this way the S4 helix would act as a voltage sensor for the channel (Greenblatt et al., 1985; Catterall, 1986; Guy and Seetharamulu, 1986; Noda et al., 1986).

The sodium and calcium channels share a structural plan consisting of four internally homologous units, each of which contains many putative hydrophobic membrane-spanning helices and the amphipathic S4 helix. In contrast, the *Shaker* protein is roughly one fourth as long as the others and contains an amino acid sequence corresponding to only one of the homology units. Because the voltage-dependent gating of A-type channels is generally similar to sodium and calcium channels (Neher, 1971), and because most known voltage and ligand-gated channels are much larger than the *Shaker* protein, it has been suggested that the *Shaker* gene codes for a subunit of a multimeric channel (Tempel et al., 1987). Previous allelic complementation experiments on A currents in pupal muscle have also suggested that more than one *Shaker* product is involved in producing a functional channel (Timpe and Jan, 1987). The expression of A-type currents in *Xenopus* oocytes injected with single *Shaker*-derived mRNA species indicates that, if the channel is multimeric, it can exist as a multimer of identical subunits (Iverson et al., 1988; MacKinnon et al., 1988; Timpe et al., 1988*a*, *b*; Zagotta et al., 1989).

An intriguing finding from molecular work on the *Shaker* gene is that alternative splicing seems to be extensive, with the potential for as many as 24 different species of mRNA capable of being produced (Kamb et al., 1988; Pongs et al., 1988; Schwarz et al., 1988). Experiments in which oocytes have been injected singly with different mRNA species have revealed A-type currents with different kinetics, differing in the macroscopic time course of onset and recovery from inactivation (Iverson et al., 1988; Timpe et al., 1988*a*, *b*; Zagotta et al., 1989).

An understanding of the molecular mechanisms of voltage-dependent gating of these channels will require detailed studies of the gating of many different channel variants, including the native channels, the channels expressed by the different mRNA species in oocytes, and channels whose structures have been altered via in vitro mutagenesis. The biophysical analysis of single-channel data can provide insight into the gating mechanism not possible with standard macroscopic voltage-clamp techniques. Statistical analysis of the open and closed durations yields detailed kinetic data on the opening and closing conformational changes of the macromolecule. These data can be compared with theoretical models to ascertain the permitted conformational states and the voltage dependence of transitions between them. The purpose of this article is to describe quantitatively the gating of single native A_1 channels and to derive a quantitative model for gating incorporating

voltage-dependent transitions among kinetically defined conformational states. This model will provide a framework for organizing and understanding the alterations in gating exhibited by structural variants of the channel.

METHODS

Drosophila Stocks

Drosophila stocks were maintained at 26°C on a cornmeal-yeast-dextrose-sucrose medium. The wild-type strain was Canton-S, and the mutant strain Sh^{KS133} was obtained from L. Salkoff of Washington University, St. Louis, MO.

Cell Culture

Cell cultures of *Drosophila* myotubes were prepared according to the procedure of Seecof (1979) (Zagotta et al., 1988). Late-gastrula stage embryos were collected and dechorionated in a 50% bleach solution for 1 min. Cells were then removed from the embryos with sharp micropipettes and dispersed onto untreated glass coverslips. The cells were allowed to differentiate in a modified Schneider's medium containing 20% heat-inactivated fetal calf serum and 8 mU/ml of insulin at 26°C. This temperature has been shown to maximize the contractile activity of myotubes in these cultures (Seecof and Donady, 1972). Many of the myotubes twitch spontaneously in the culture medium or in physiological saline solutions containing 2 mM Ca^{++}, and nearly all of them exhibit a pronounced and prolonged contracture when exposed to a solution containing high K^+ (140 mM) and Ca^+ (2 mM).

Electrophysiology

Electrophysiological recordings were done 8–24 h after plating of the cells. The cell membranes were voltage-clamped and current was recorded with a List EPC-7 patch clamp amplifier (List Medical/Medical Systems, Greenvale, NY). The output of the amplifier was low-pass filtered through an 8-pole Bessel filter (Frequency Devices, Inc., Haverhill, MA), digitized at the frequencies indicated in the figure legends, and stored for later analysis. A Digital Equipment Corp. LSI 11/73-based minicomputer system (Indec Systems, Sunnyvale, CA) controlled the voltage-clamp protocols, and was used for data analysis.

The pipette potential was nulled just before seal formation. The voltage error due to junction potentials was estimated to be <5 mV based on the reversal potential of potassium channels recorded in experiments done in solutions with symmetrical K^+ concentrations. No correction was made for this error.

For whole-cell recordings, electrodes with input resistances of 1–2 MΩ in standard solutions were used. The input resistance of the cells was usually >2 GΩ. Typically, for currents >200 pA, 50–80% of the series resistance was electronically compensated. For currents <1 nA, the largest outward current considered in these experiments, the maximum uncompensated voltage error is 4 mV, assuming a series resistance of 4 MΩ, two to four times the pipette resistance. Most of the capacitative current was subtracted electronically using the capacitance compensation circuitry of the patch clamp. The remaining uncompensated capacitative current and ohmic leak current were digitally subtracted from the data using leak templates scaled to the appropriate voltages. The leak templates were constructed by fitting smooth functions to the average current response to 20-mV depolarizing steps from a holding potential of −70 mV. No time-dependent currents were activated in this voltage range.

Single-channel currents were recorded primarily from cell-attached patches although some outside-out patches were used (Hamill et al., 1981). Voltage steps were delivered every 5 s. Linear leak and uncompensated capacitative currents were digitally subtracted using leak

templates made from sweeps with no openings. For the ensemble averages and duration histograms, the single-channel data were idealized using a 50% amplitude criterion to detect opening and closing transitions. The ensemble averages that have been expressed in probability units were determined by dividing the current averages by the number of channels in the patch (one for all of the patches reported here) and the unitary current amplitude. The adequacy of theoretical fits to data was determined by eye. The results presented are characteristic for a bandwidth ≤2 kHz. There may be faster transitions that were unresolved at this bandwidth.

Solutions

For whole-cell and outside-out experiments the composition of the solutions were as follows (in millimolar): external (bath) 140 NaCl, 2 KCl, 6 $MgCl_2$, 5 HEPES, pH 7.1; and internal (pipette) 140 KCl, 2 $MgCl_2$, 11 EGTA, 10 HEPES, pH 7.1. For some whole-cell and outside-out experiments internal 140 mM KCl was replaced by 70 mM KCl and 70 mM KF, and external 6 mM $MgCl_2$ was replaced by 4 mM $MgCl_2$ and 2 mM $CaCl_2$. Under these conditions no marked differences in the kinetics or voltage dependence of the A current were observed. For cell-attached experiments the external solution was used in the pipette and the internal, high K^+ solution was used in the bath. In this high K^+ solution the cell resting potential should be close to 0 mV and therefore the voltages reported are close to the actual voltage across the membrane. No obvious differences were seen in the voltage dependence for any of the channels between cell-attached and cell-free patches, although there was a tendency for channels in cell-free patches to open more times during a voltage step. The free Ca^{++} concentration of the internal solution was estimated to be ~1–10 nM. The temperature of the recording chamber was controlled at 22 ± 0.2°C.

RESULTS

The general macroscopic properties of *Shaker* A-type channels are illustrated by a family of whole-cell current records from a cultured wild-type myotube (Fig. 1 *A*). Outward currents were recorded from this cell after 12 h in culture, a developmental stage that had similar proportions of A-type and delayed outward currents (Zagotta et al., 1988). Outward currents become evident at steps to −30 or −20 mV. As steps are made to more positive voltages, the currents inactivate faster. The transient current was absent in myotubes cultured from animals homozygous for Sh^{KS133}, a null mutant of the *Shaker* locus (Fig. 1 *B*), leaving only outward currents that do not inactivate on the time scale of these voltage pulses. Macroscopic A-type potassium currents that are altered by mutations of the *Shaker* gene have also been recorded from pupal and larval muscle (Salkoff, 1983; Wu and Haugland, 1985). The transient current develops earlier than the sustained current during both embryonic (Zagotta et al., 1988) and pupal (Salkoff and Wyman, 1981*a*) development. In embryonic myotubes, even at early times when the sustained current is relatively small, its contribution to total outward current is significant, and the A current is not completely isolated. Because of this, it is difficult to determine in whole-cell measurements how much of the sustained current is due to a noninactivated fraction of the A current. In principle, pharmacological experiments could be used to determine the extent of steady-state A current but common potassium channel blockers, such as 4-aminopyridine, are not totally specific for A currents in these cells. Single-channel measurements from cell-attached patches have indicated that

inactivation of these A-type channels is nearly complete after 10 ms at voltages above 0 mV (Zagotta et al., 1988).

Inactivation of the macroscopic A currents occurs over a range of −40 to −20 mV (Fig. 2). Fig. 2 *A* shows a family of currents recorded after 500-ms prepulses to voltages between −50 and −20 mV. The normalized peak current during the test pulse is plotted against prepulse potential for seven cells in Fig. 2 *B*. To partially correct for contamination by delayed current, we subtracted the current 50 ms after the start of the pulse from the current at the time of the peak of the large transient currents. This correction assumes that delayed current is nearly completely activated at the time of the peak of the A current at +50 mV (the test pulse potential) and is negligibly inactivated by 500-ms prepulses over the range the A current is inactivated. Prepulse inactivation experiments on Sh^{KS133} myotubes have suggested that

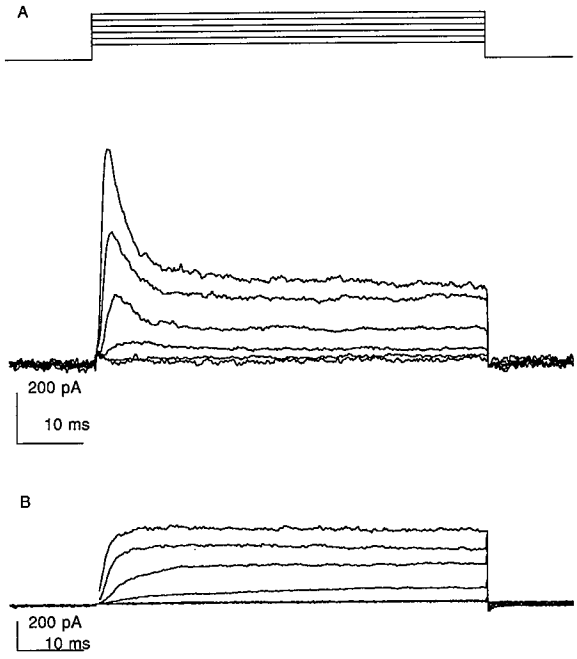

FIGURE 1. Whole-cell currents in cultured embryonic myotubes from wild-type (*A*) and Sh^{KS133} mutant (*B*) *Drosophila*. The membrane potential was stepped from a holding potential of −70 mV to a prepulse potential of −100 mV for 500 ms and then depolarized for 60 ms to command potentials between −50 and +50 mV in 20-mV increments. The voltage pulse protocol is shown at the top. The data were filtered at 2 kHz and digitized at 100 μs per point.

both of these assumptions are valid (data not shown). The points have been fitted with the voltage-dependent proability of remaining activatable [$P(V)$] derived from the Boltzmann distribution:

$$P(V) = \frac{I}{I_{max}} = \frac{1}{1 + e^{[(v - v_{1/2})/Y]}} \quad (1)$$

The midpoint for inactivation ($V_{1/2}$) is −29 mV, and the slope factor (Y) is 3.5 mV. The midpoint of inactivation is more positive than most other A-type currents (Connor and Stevens, 1971; Thompson, 1977; Cooper and Shrier, 1985; Kasai et al., 1986; Taylor, 1987) including the A_2 current that is found in *Drosophila* neurons (Solc et al., 1987, Solc and Aldrich, 1988).

Gating Kinetics of Single A_1 Channels

Whole-cell A current kinetics change markedly between −20 and +50 mV (see Fig. 1). At less positive voltages, the macroscopic currents turn on more slowly and inactivate much more slowly. Although detailed descriptions of this voltage-dependent gating require the development of kinetic models that can fit all of the macroscopic and single-channel measurements (see next section), many important conclusions can be drawn from analysis of single-channel behavior without a complete kinetic model. In this section, we analyze the statistical distributions of single-channel open and closed events and their voltage dependence. Although our experiments were limited by the tendency of channels to disappear from patches after a few minutes

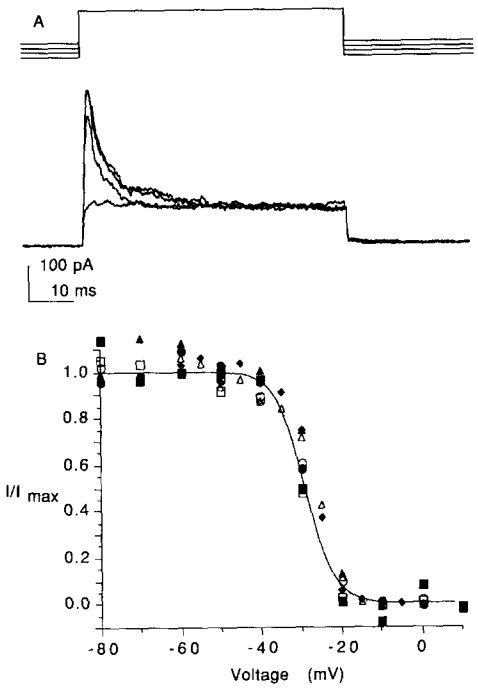

FIGURE 2. Effects of prepulse potential on the whole-cell currents. (*A*) Whole-cell currents elicited by steps to +50 mV after a 500-ms prepulse to −50, −40, −30, and −20 mV from a holding potential of −70 mV. The voltage pulse protocol is shown at the top. The data were filtered at 2 kHz and digitized at 100 μs per point. (*B*) Prepulse inactivation curve for the whole-cell A currents. Normalized peak A current during the step to +50 mV is plotted vs. prepulse potential. The normalized A current was calculated by subtracting the current 50 ms after the start of the pulse from the current at the time of the peak of the large transient currents. The different symbols represent data from seven different myotubes. The data are fitted by a Boltzmann distribution (Eq. 1) with a slope (Y) of 3.5 mV and a half-inactivation voltage ($V_{1/2}$) of −29 mV.

(Zagotta et al., 1989), they were facilitated by the high probability of obtaining patches with only a single channel.

Representative single-channel currents at −20, 0, +30, and +50 mV are shown in Fig. 3. The openings occur in short bursts of only a few opening events. A burst is defined as any group of openings that are separated by closed times of duration less than a burst criterion duration. This criterion was determined by examining closed-duration distributions (data not shown) and set to 1 ms, approximately four times the fastest component of the closed durations. Often only one burst occurs during a voltage step, although multiple bursts, separated by closed intervals that are long compared with closed durations during a burst, can occur. The occurrence of a

burst of openings essentially divides the current record into three segments: the time before the first opening of the burst, the burst itself, and the period after the burst. The time after the burst either contains additional bursts or a long-lasting closed duration that continues until the end of the record. We have analyzed the bursts of openings to determine the voltage dependence of the number of bursts per record, the open durations, the number of openings per burst, the closed duration within bursts, the latency until first opening (first latency), and the probability of observing a record with no opening (a blank record).

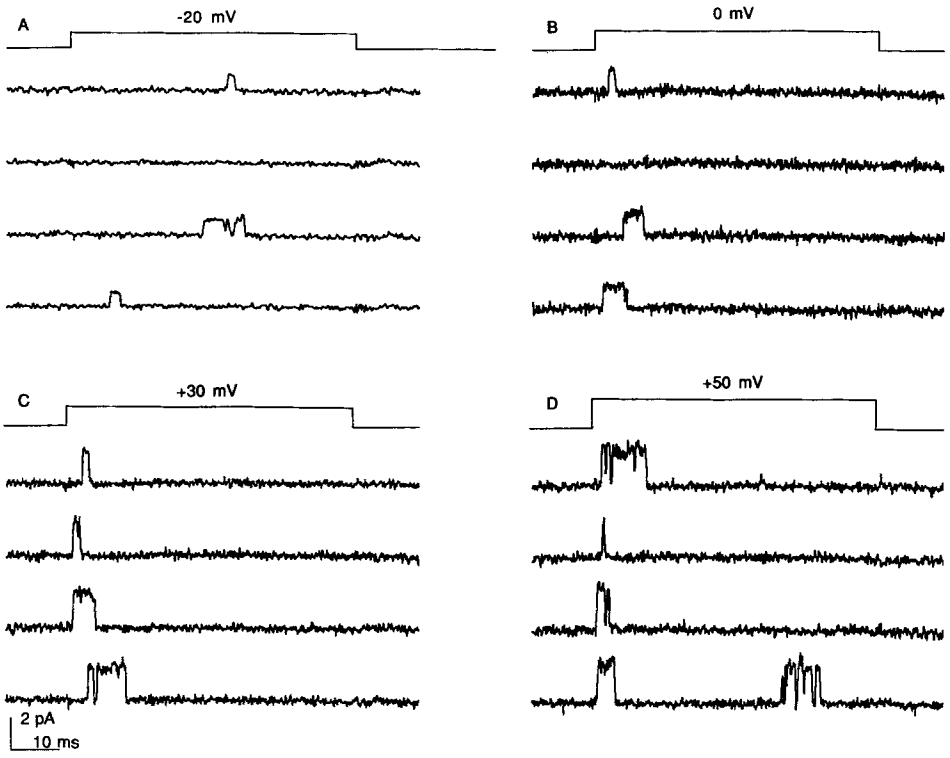

FIGURE 3. Representative openings of a single A_1 channel at -20 mV (*A*), 0 mV (*B*), $+30$ mV (*C*), and $+50$ mV (*D*). The channels were recorded from a cell-attached patch. The voltage protocol is shown at the top. The data were filtered at 1 kHz (*A*) or 2 kHz (*B*, *C*, *D*), and digitized at 50 μs per point.

The channels showed a marked tendency to give only a single burst during a voltage step. Fig. 4 shows the mean number of bursts per record, given the occurrence of at least one burst, for four cell-attached patches over a voltage range from -20 to $+50$ mV. Over the entire voltage range there is little tendency to burst more than once. The lack of voltage dependence in the number of bursts cannot account for the pronounced voltage dependence of the macroscopic currents.

Because channels rarely open into additional bursts, the long closed state can be identified as an inactivated state. This indicates that there are at least two closed

states of the channel. Two possibilities exist for transitions among these states during a burst:

$$C \underset{\delta}{\overset{\gamma}{\rightleftharpoons}} O \xrightarrow{\kappa} I \qquad \text{(Scheme 1)}$$

or

$$O \underset{\gamma}{\overset{\delta}{\rightleftharpoons}} C \xrightarrow{\kappa} I \qquad \text{(Scheme 2)}$$

In both cases a burst comes about by transitions between the open state and the short-duration closed state and is terminated by a transition to the long-duration inactivated state. Although we cannot definitely distinguish between the two schemes, we consider scheme 1 to be preferable for these inactivating channels. Scheme 2 would require an additional pathway into the open state for the channel to activate from rest and therefore an additional closed state. Scheme 1 is consistent

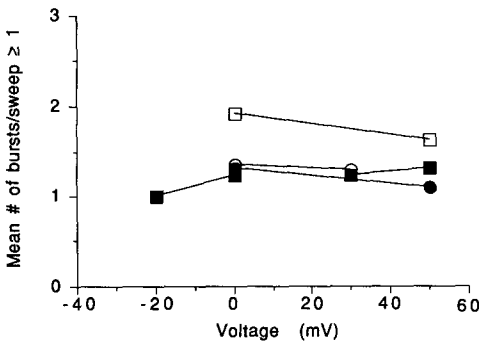

FIGURE 4. Voltage dependence of the number of bursts per voltage pulse given at least one burst. The mean number of bursts during a 60-ms voltage pulse is plotted against the pulse potential. The mean was determined after omitting records with no openings. The criterion for burst termination was a closure of more than 1 ms. The different symbols represent data from four different single-channel cell-attached patches.

with the observation that the closed durations within the bursts are never longer than the first latencies (see below). All of the qualitative conclusions about voltage dependence in the following analysis apply equally well to both kinetic schemes. In keeping with a desire to use as few states as possible, we will use scheme 1 as a beginning model for the interpretation of the data on single-channel kinetics.

According to scheme 1, the distribution of open durations will be a single exponential with a mean duration of $1/(\delta + \kappa)$. The open durations are well described by this distribution, as can be seen by the open-duration histograms in Fig. 5, *A* and *B*. Open duration histograms at -20 and $+50$ mV are well fitted by single exponential probability density functions with means of 1.5 ms. The lack of any appreciable voltage dependence in the mean open duration between -20 and $+80$ mV is shown for six patches in Fig. 5 *C*. These results suggest the channel contains a single open state for which the sum of the closing rates $(\delta + \kappa)$ does not depend on membrane potential.

According to this scheme, an open channel will either terminate a burst with a probability of $\kappa/(\delta + \kappa)$, or reenter the burst with a probability of $\delta/(\delta + \kappa)$. The

number of openings in a burst (n) will be described by a geometric distribution:

$$P(n) = (1 - q)^{(n-1)}q, \tag{2}$$

for ($n = 1, 2, 3 \ldots$), where q is the probability of termination of a burst and is equal to $\kappa/(\delta + \kappa)$. Fig. 6, *A* and *B* show histograms of the number of openings per burst at -20 and $+50$ mV. Geometric distributions (Eq. 2) are shown by the large circles and fit well with q equal to 0.40 at -20 mV and 0.49 at $+50$ mV. The lack of any appreciable or consistent voltage dependence in the number of openings per burst between -20 and $+80$ mV is shown for five patches in Fig. 6 *C*. The q values from different patches range from 0.4 to 0.9, suggesting that κ is generally similar to or larger than δ. The analysis of open durations and number of openings per burst

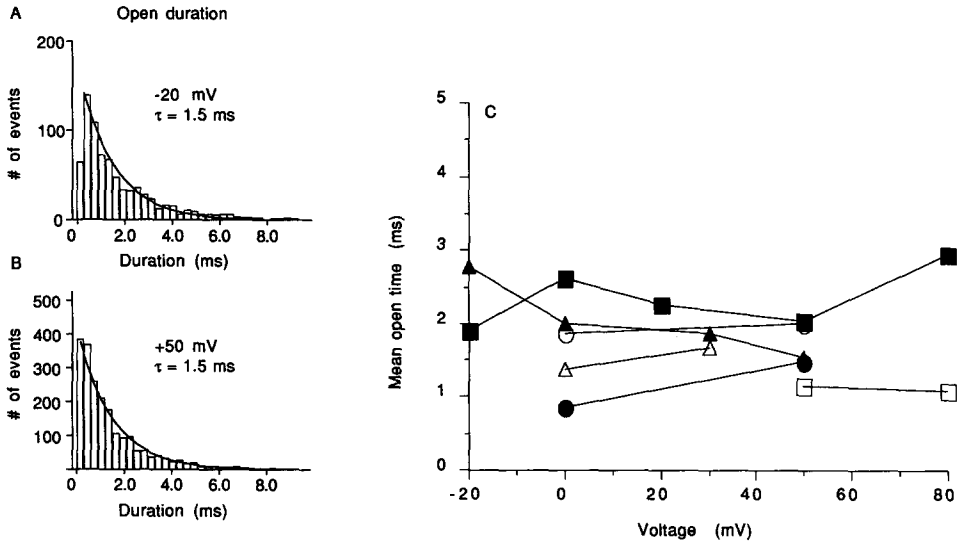

FIGURE 5. Voltage dependence of open durations. (*A*) A frequency histogram of the open durations during voltage steps to -20 mV. The histogram is fitted by a single-exponential function with a time constant of 1.5 ms. The shortest bin was not considered in the fits. The bin size is 300 μs. (*B*) A frequency histogram of the open durations during voltage steps to $+50$ mV, fitted by a single-exponential function with a time constant of 1.5 ms. The bin size is 300 μs. (*C*) The mean open duration is plotted vs. the step potential. The different symbols represent data from six different patches.

indicates that neither the mean open duration $[1/(\delta + \kappa)]$ nor the probability of terminating a burst $[\kappa/(\delta + \kappa)]$ depend on membrane potential. Therefore δ and κ themselves do not depend on membrane potential. This means that no appreciable charge is redistributed across the membrane between state O and either of the transition states to states C or I.

The minimum number of closed states within a burst can be determined by the number of exponential components in the distribution of closed times within a burst. Measured distributions of burst closed durations were well fitted with single exponential functions with means of 0.28 ms at -20 mV (Fig. 7 *A*) and 0.25 ms at $+50$ mV (Fig. 7 *B*). The durations are very fast and the fastest bins are severely

attenuated by bandwidth limitations and therefore not considered in the fits. These results indicate that a burst has a high probability of containing sojourns into a single closed state with a lifetime of a few hundred microseconds. The fact that the burst closed durations are much shorter than the first latencies at all voltages (−20 to +50 mV; see below) is consistent with closing to a state that is traversed on the activation pathway. If this is true the result also indicates that bursts have a low probability of including sojourns to more than one of the closed states that the channel passed through along the way to opening, at least at voltages positive to −20 mV.

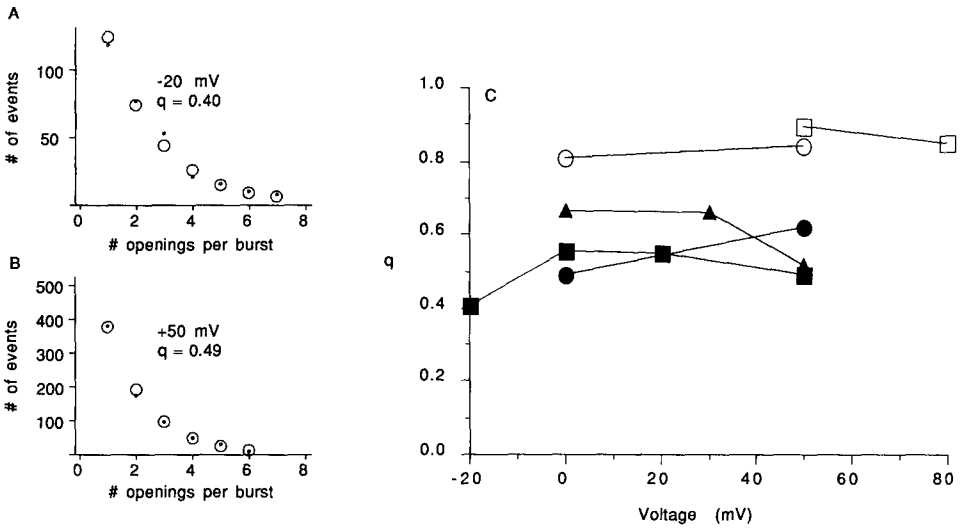

FIGURE 6. Voltage dependence of number of openings per burst. (*A*) A frequency histogram of the number of openings per burst during voltage steps to −20 mV is represented as small dots. The histogram is fitted by a geometric distribution (Eq. 2), represented by circles around the dots, with the probability of terminating the burst (q) equal to 0.40. The criterion for burst termination was a closure of more than 1 ms. (*B*) A frequency histogram of the number of openings per burst during voltage steps to +50 mV, fitted by a geometric distribution with the probability of terminating the burst (q) equal to 0.49. (*C*) The probability of terminating a burst (q) is plotted vs. the step potential. The different symbols represent data from five different patches.

The lack of appreciable voltage dependence in the mean burst closed durations is shown for five patches between −20 and +80 mV in Fig. 7 *C*. This lack of voltage dependence indicates that the transition rate from the burst closed state to the open state (γ) is not voltage dependent. Therefore no appreciable charge redistribution across the membrane occurs between the burst closed state and the transition state to opening. We have already found that the rate for entering the burst closed state from the open state (δ) is not voltage dependent. If the burst closed state is in the opening pathway, these results mean that the final opening step is not measurably voltage dependent. Finally, since we determined that the inactivation transition (κ) is voltage independent, and returns from inactivation (λ) are rare and probably volt-

age independent (Fig. 4), all of the transitions that the channel undergoes after first opening are independent of membrane potential.

In contrast to the transitions made after opening, some or all of the transitions made before first opening are highly dependent upon membrane potential. Distributions of first latencies are shown in Fig. 8 *A* for voltage steps to −20, 0, +20, and +50 mV. The distributions illustrate that first openings occurred quite late after the voltage step at less positive voltages, and became considerably faster at more positive voltages. The delay in the distributions (particularly evident in the −20-mV distribution) indicates that more than one closed state must be traversed before the

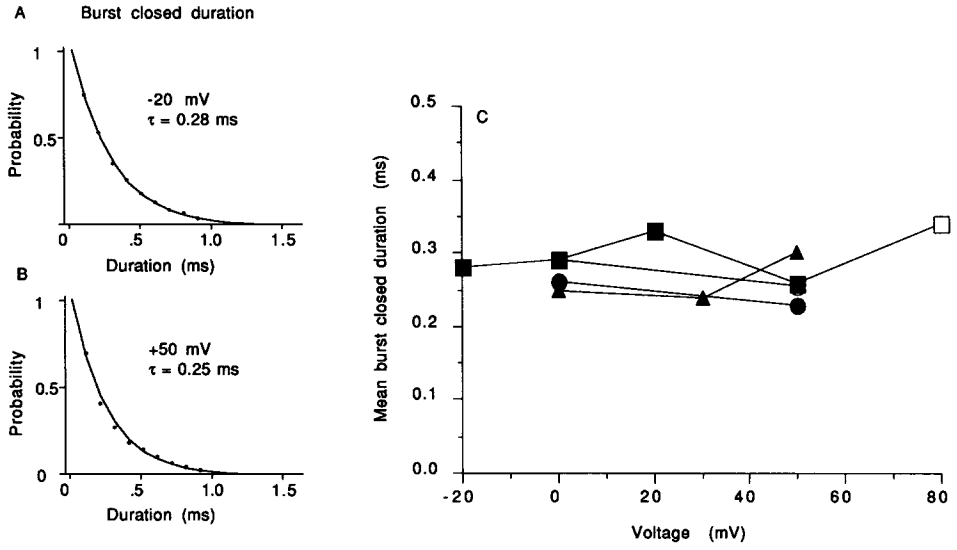

FIGURE 7. Voltage dependence of burst closed durations. (*A*) A tail distribution of the burst closed durations during voltage steps to −20 mV. Tail distributions describe the probability of a closure being longer than the duration on the abscissa and are calculated as 1 minus the cumulative distribution. The histogram is fitted by a single-exponential function with a time constant of 0.28 ms. The criterion for burst termination was a closure of more than 1 ms. (*B*) A tail distribution of the burst closed durations during voltage steps to +50 mV, fitted by a single-exponential function as in (*A*) with a time constant of 0.25 ms. (*C*) The mean burst closed duration is plotted vs. the step potential. The different symbols represent data from five different patches.

channel opens. The times at which the first latency distributions cross 50% of their final value (the median first latency) are plotted against membrane potential between −20 and +80 mV for four patches in Fig. 8 *B*. The median first latency changes sevenfold over this voltage range indicating a large voltage dependence for at least some of the transition rates among the closed states traversed on the way to opening.

At lower voltages the first latency distributions frequently reach a plateau probability that is much less than 1 because of records that elicited no openings (blank records). This is not because the pulse was too short compared with the opening

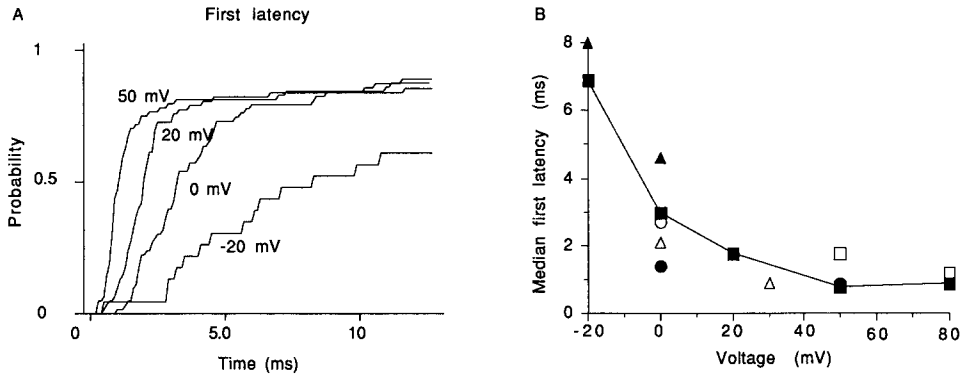

FIGURE 8. Voltage dependence of latencies to first opening. (*A*) Cumulative distributions of first latencies during voltage steps to −20, 0, +20, and +50 mV. (*B*) The median first latency is plotted vs. the step potential. The different symbols represent data from six different patches.

rates, as longer records did not elicit additional openings. The probability of observing a blank record is plotted against membrane potential for five cell-attached patches in Fig. 9. Blank records were fairly common at −20 and 0 mV, but were less likely at +50 mV. A fairly large amount of variability exists among patches in the occurrence of blank records. The blank records could conceivably come about in two ways: (*a*) channels are unavailable for opening because of their residing in an inactivated state at the beginning of the voltage pulse or (*b*) channels are available for opening, but inactivate during the pulse before opening. The proability of observing a blank was small at +50 mV, indicating that the channel was available for opening at the beginning of the voltage step and that blank records at 0 mV resulted from inactivation before opening. This is consistent with schemes in which closed-state inactivation rates decrease with membrane potential or where closed-state inactivation rates are independent of membrane potential, but the dwell time in inactivatable closed states decreases with membrane potential. This latter idea is consistent with the faster first latencies at higher voltages. The variability in the probability of obtaining a blank record from patch to patch probably indicates a variability in the rate of closed state inactivation.

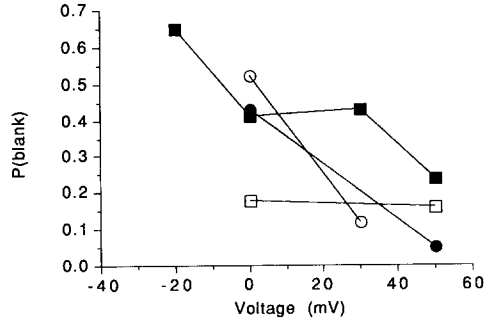

FIGURE 9. Voltage dependence of the probability of a blank record. The fraction of records that exhibited no openings during 60-ms steps to the membrane potential on the abscissa are plotted vs. the step potential. The different symbols represent data from four different patches.

A Kinetic Scheme for A_1 Channel Gating

The analysis of open durations, burst parameters, and first latencies has demonstrated that all of the transitions after first opening, including the inactivation transition, are independent of voltage, and that all of the voltage dependence of the macroscopic currents arises from voltage-dependent first latencies. In this section we will formulate a quantitative description of voltage-dependent gating of A_1 channels, based on the previous conclusions, and compare its predictions to macroscopic and single-channel data.

A successful kinetic model for a voltage-gated ion channel must include a diagram of closed, open, and inactivated states with allowed transitions between states, and specification of voltage dependence for each of the permitted transition rates. Calculations based on the model must reproduce all of the measurable macroscopic and single-channel kinetics over the entire voltage range over which gating occurs.

We have made the following assumptions in developing models for gating. Although the validity of these assumptions cannot be shown from our data, some of them are supported by experimental evidence. Each assumption is followed by lines of evidence motivating and supporting it.

Gating can be described by a time-homogeneous Markov process. Markov models are generally used, and we have no data that suggest that they are not valid for this channel (see French and Horn, 1983 for a discussion of the applicability of Markov models).

The channel reaches equilibrium among the states in the model during the 500-ms prepulses used to measure the voltage dependence of resting inactivation. This assumption simplifies the fits of models to the resting inactivation curve. It is supported by the fact that models that fit all of the kinetic and voltage-dependence data reached equilibrium in <500 ms during steps to the standard prepulse voltages (data not shown). In addition, longer prepulses caused only a minor hyperpolarizing shift in the measured prepulse inactivation curve.

Activation comes about by the independent movement of identical charges. This is the simplest assumption about activation kinetics. It constrains rate constants for transitions between resting closed states to be integral multiples of the first order transition rates α and β (see Armstrong, 1969) and therefore greatly reduces the number of rate constants that must be specified. We were influenced in making this assumption by the results obtained in *Shaker* mRNA-injected *Xenopus* oocytes and by the similarity in voltage dependence between *Shaker* A channels and sodium channels (Aldrich et al., 1983; Iverson et al., 1988; MacKinnon et al., 1988; Timpe et al., 1988*a*, *b*; Zagotta et al., 1989). Because A currents can be expressed in oocytes injected with a single mRNA species that codes for a protein one-fourth the size and homologous to one of the four repeated units of the sodium channel, it seems that the A channel operates in oocytes as a multimer of identical subunits. We do not know the subunit composition of the channels in muscle cells, but the similarity of currents in oocytes and muscle suggests that gating operates by similar mechanisms (see Zagotta et al., 1989).

Closed state inactivation rates are not voltage dependent. We have shown above that the rate of inactivation from open states is independent of membrane potential. The

simplest assumption is that any closed state inactivation is also voltage independent.

Closings during bursts are to preopen (resting) closed states. This assumption is consistent with the duration of the burst closed times always being less than the first latencies. It is possible that burst closings occur by a process that is independent of the opening pathway. A specific case of this would be open channel block by an endogenous blocking particle. As discussed for scheme 2, this would require an additional pathway into the open state for the channel to activate from rest and therefore an additional burst closed state.

Rate constants depend exponentially on membrane potential. This would be expected for the simplest case of a first-order gating transition that rotates an effective dipole, or moves charge through the membrane, between states. The voltage dependence of the activation rates were therefore constrained by the following equations:

$$\alpha(V) = A_\alpha e^{(v/v_\alpha)} \qquad \text{and} \qquad \beta(V) = A_\beta e^{-(v/v_\beta)} \tag{3}$$

where A_α and A_β are the rates at 0 mV of α and β, respectively, and V_α and V_β specify their voltage dependencies. Other forms of voltage dependence are possible (see Stevens, 1978), but require specification of the functional form and parameters of the voltage dependence of each rate constant, and therefore greatly increases the arbitrary parameters in the model. For the activation rate constant (α), the exponential assumption seems to hold well above 0 mV (see below).

These assumptions are simple and reduce considerably the number of free parameters that must be specified to construct a model. We have used the following basic strategy for formulating and testing specific models. The rate constants for transitions directly into and out of the open state at all voltages were determined from the open duration and burst analysis as detailed above. After this, an equilibrium formulation of the model was used to fit the resting inactivation curve measured from whole-cell experiments. For the general model shown below:

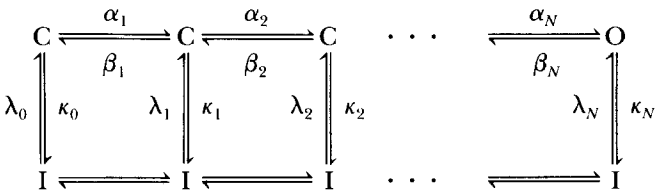

(Scheme 3)

The equilibrium probability of residing in a noninactivated state as a function of membrane potential [$P(V)$] is given by the following equation:

$$P(V) = \frac{1 + \sum_{j=1}^{N}\left[\prod_{i=1}^{j}\left(\frac{\alpha_i}{\beta_i}\right)\right]}{1 + \sum_{j=1}^{N}\left[\prod_{i=1}^{j}\left(\frac{\alpha_i}{\beta_i}\right)\right] + \frac{\kappa_0}{\lambda_0} + \sum_{j=1}^{N}\left[\prod_{i=1}^{j}\left(\frac{\alpha_i}{\beta_i}\frac{\kappa_j}{\lambda_j}\right)\right]} \tag{4}$$

For models with activation rate constants α and β exponentially dependent on volt-

age and representing the independent action of identical subunits:

$$\frac{\alpha}{\beta} = K(V) = \frac{A_\alpha}{A_\beta} e^{[V(1/V_\alpha + 1/V_\beta)]} \quad (5)$$

From these fits we determined the equilibrium constant for the activation transition of each subunit [$K(V)$] at 0 mV (A_α/A_β) and the voltage dependence of the equilibrium ($1/V_\alpha + 1/V_\beta$). Next the first latency distributions were fitted with numerical solutions of the model to determine the absolute magnitudes and voltage dependence of the activation and deactivation rates. Finally, numerical solutions of the model were used to calculate macroscopic currents and then they were compared with the single-channel ensemble averages and the whole-cell currents. Peak conductance and time to peak current of the calculated currents were compared with their counterparts from the whole-cell currents.

Number of Inactivated States

While multiple bursts are sometimes observed during short voltage pulses, the channel rarely, if ever, reopens during maintained depolarizations. This suggests that there is a second, absorbing, inactivated state from which reopening cannot occur. Slow inactivation processes are also evident in prepulse inactivation experiments in which very long prepulses (5 s) result in small (8 mV) hyperpolarizing shifts in the resting inactivation curves. In addition, both the whole-cell and single-channel currents exhibit a rundown phenomenon, even in cell-attached patches, and a double exponential recovery from inactivation time course, which may be related to additional inactivated states. The rundown phenomenon makes experiments on slow inactivation and recovery extremely difficult. This slow inactivation process is slow compared with the fast gating processes considered here and therefore will be disregarded in the following development of a kinetic model. Because slow inactivation influences the time course of recovery determined in a two-pulse experiment, we have not tried to fit recovery time courses.

Number of Closed States

A minimum number of resting closed states can be determined by fitting the first latency distribution functions with the predictions of models with different numbers of closed states. Fig. 10 *A* shows fits of first latency distributions obtained at 0, +20, and +50 mV with the predictions of a model as follows:

$$\mathrm{C} \xrightarrow{4\alpha} \mathrm{C} \xrightarrow{3\alpha} \mathrm{C} \xrightarrow{2\alpha} \mathrm{C} \xrightarrow{\alpha} \mathrm{C} \xrightarrow{\gamma} \mathrm{O} \quad \text{(Scheme 4)}$$

Channels are assumed to reside in the left-most closed state at the beginning of the voltage pulse. Scheme 4 fits well with five closed states (shown). Reasonable fits can be obtained with three or more closed states. Fits are much less adequate with two closed states. It is difficult to establish an upper limit for the number of states in the opening pathway. Because of the constraint of opening rates being integral multiples of α, adding more closed states does not seriously affect the amount of delay in the calculated first-latency distributions. For these fits we have not assumed anything about the voltage dependence of the rate constants α and β, but have adjusted

α independently at each membrane potential to determine the best fit. We ignored any contribution of β because we are fitting first-latency functions at high voltages where the backward rates are likely to be negligible. Incorporating values for β arrived at in the full analysis presented below did not affect the voltage dependence of α (see below). The value for γ was determined from the analysis using scheme 1 and is independent of voltage. The values of α found by fitting the first-latency distributions vary exponentially with membrane potential (Fig. 10 *B*). This provides some support for the assumption of exponential voltage dependence of the activation rate constants (Eq. 3).

Closed State Inactivation

It is clear from the absence of a large fraction of blank records at +50 mV that the channels are available for opening essentially every trace (Fig. 9), indicating that

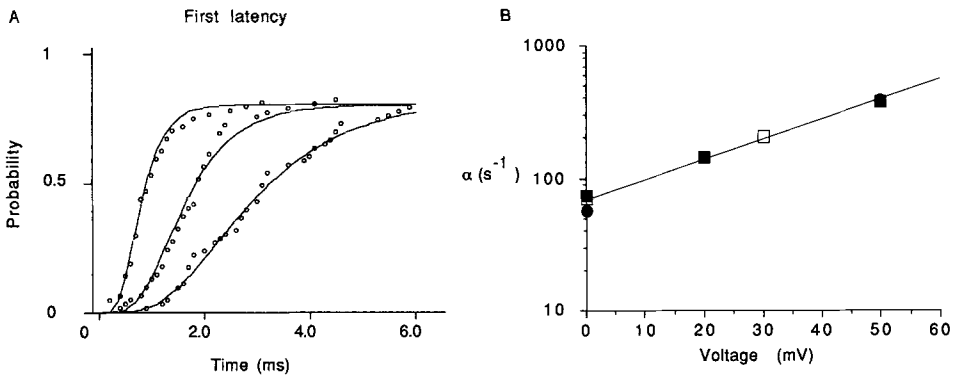

FIGURE 10. Exponential voltage dependence of activation rates. (*A*) Distribution of first latencies during voltage steps to 0, +20, and +50 mV are plotted as dots. These data are fitted by numerical solutions to scheme 4 for each membrane potential. (*B*) The values of α from these fits are plotted vs. the step potential on semi-log axes. The different symbols represent data from four different patches. These data are fit by an exponential (Eq. 3) with an amplitude (A_α) of 700 s^{-1} and a voltage dependence (V_α) of 27 mV.

closed-state inactivation is not appreciable at +50 mV. At 0 mV, however, there is a higher probability of obtaining a blank record. This voltage-dependence of the probability of blank records indicates that pathways are present for inactivating from closed states without first opening, and thus discounts fully coupled models of gating where opening is a prerequisite for inactivation. The simplest conclusion is that inactivation is possible from some closed states and is more effective at lower voltages because the opening process is slow, increasing the probability that inactivation will occur before opening. This would arise if inactivation could occur from a few of the closed states but is not voltage dependent.

Classes of Models

We have considered three general classes of models for A_1 channel gating: (*a*) independent activation and inactivation, (*b*) independent subunits that can each activate

and inactivate, (*c*) coupled models where at least some of the gating transitions arise from the entire molecular assembly and not from individual subunits.

Independent activation and inactivation. This class of models incorporates separate and independent transitions for activation and inactivation. It is exemplified by the Hodgkin and Huxley model for sodium channel gating (Hodgkin and Huxley, 1952). Similar models have been proposed for A-type channels from macroscopic currents (Neher, 1971; Connor and Stevens, 1972). In this class of models, inactivation begins immediately upon a step change in membrane potential and takes place independently of the activation process. Activation and inactivation are separately voltage dependent. A simple molecular view of this type of model would incorporate a number of subunits responsible for activation and a separate one responsible for inactivation. In independent models, closed state inactivation must proceed with the same rate regardless of the state of activation. A model with independent activation and inactivation can be expressed as the following kinetic scheme:

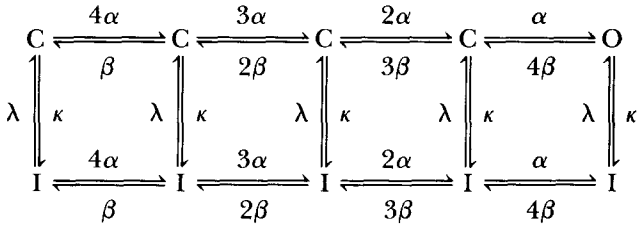

(Scheme 5)

Independent activation and inactivation processes are not consistent with the single-channel data. For channels with highly voltage-dependent macroscopic inactivation, scheme 5 demands that either the mean open duration or the number of openings per burst be voltage dependent. We have shown that neither of these measurable quantities is voltage dependent between −20 and +80 mV (Figs. 5 and 6) and have concluded therefore that inactivation of open channels is not voltage dependent. If inactivation occurs equally well from any closed state, as required by scheme 5, and is independent of membrane potential, as required by the single-channel data, then there can be no voltage dependence of resting inactivation. This is clearly not the case (see Fig. 2). This type of scheme is also incompatible with the general lack of blank records at more positive voltages, indicating that most channels open before inactivating at these voltages, even though macroscopic inactivation is very fast.

Independent subunits, each with activation and inactivation. This class of model is inspired in part by the results in *Xenopus* oocytes that suggest that the channel can exist as a multimer of identical subunits. In this formulation, each of the subunits acts independently, inactivating only after it activates:

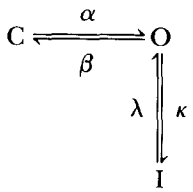

(Scheme 6)

A channel can be open only when all of the subunits are in the O state but will be inactivated when any of the subunits are in the I state. Because of our single-channel results, the transitions between C and O would be voltage dependent whereas the O to I transitions would be independent of membrane potential. A molecular view of such a model would involve redistribution of charge across the membrane as a subunit enters the O conformation and becomes activatable. Any subunit could then inactivate by a mechanism that does not redistribute charge in the membrane, perhaps by a block of the activatable state by a part of the subunit that serves as a plug of the open channel, similar to the model of Armstrong and Bezanilla (1977) for sodium channels. Each subunit has both activation and inactivation "gates." Because the inactivating process cannot occur until the subunit activates, each subunit is absolutely coupled. The multisubunit model that arises from several independent absolutely coupled subunits is not absolutely coupled, however, as inactivation can occur in some of the subunits before all of the subunits are in the O state. An expanded state diagram for a channel consisting of four subunits operating accord-

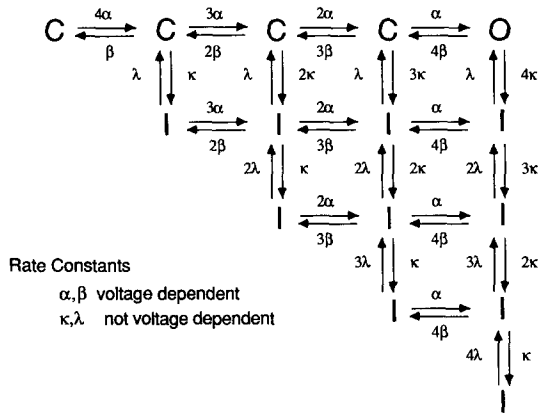

FIGURE 11. Model representing the independent conformational change of four subunits, each with a coupled activation and inactivation transition according to scheme 6. The activation transition rates (α and β) are voltage dependent while the inactivation transition rates (κ and λ) are independent of membrane potential. The channel is open if all of the subunits are in the activated conformation and inactivated if any of the subunits are in the inactivated conformation.

ing to scheme 6 is shown in Fig. 11. Adding additional subunits will add states along the lower diagonal and change the multipliers on some of the rate constants. Although such a model has many states, the rate constants are constrained to be integral multiples of the elementary rate constants for activation (α and β) and inactivation (κ and λ) of the individual subunits.

This class of models is attractive for several reasons. The subunits act independently and identically, in keeping with the presumed expression of homomultimers in the oocytes. The complete model contains partially coupled activation and inactivation processes, intermediate between absolute coupling and independence. The inactivation rates accelerate as activation progresses, therefore resulting in voltage-dependent closed-state inactivation. In addition, the model has a large number of inactivated states, which may account for some of the complexities of slow inactivation.

We have performed extensive calculations with this scheme and compared its pre-

dictions to the single-channel and macroscopic data. Although the model can do quite well in fitting subsets of the macroscopic and single-channel data, it is clearly inadequate for fitting all of the data over the entire voltage range. The following problems were evident:

(*a*) The model predicts too much voltage dependence of the mean open durations. This is because of the voltage dependence of β needed to fit the resting inactivation curve. Because the final closing rate is actually 4β, the problem of voltage dependence of the open durations is severe. The open duration could conceivably be voltage independent if 4β and 4κ changed together such that $1/(4\beta + 4\kappa)$ was not a function of membrane potential, but this would give a voltage-dependent number of openings per burst which is also not observed.

(*b*) While the measured burst closed durations have a mean of ~0.3 ms independent of membrane potential over the range −20 to +50 mV, the model predicts durations with a mean of 0.3 ms at +50 mV, increasing to 1.7 ms at 0 mV.

(*c*) The model produces too much closed-state inactivation. Inactivation from closed states is very prominent in this independent subunit model because of the ability of many closed states to inactivate. This predicts a large fraction of blank records at high voltages, a very negative resting inactivation curve, or extremely large α and β rates which remove much of the delay seen in the first latency distribution.

Although quite nice fits could be obtained to the macroscopic data, no amount of manipulation of rate constants or gating charge could make the independent subunit model fit all of the single-channel and macroscopic data well. The inadequacies of the model indicate that a mechanism involving independent subunits, each of which can open and then inactivate, is not tenable for the *Shaker* A-type channels. The problems are not alleviated if the individual subunits are allowed to inactivate from closed states:

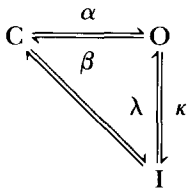

(Scheme 7)

This model does even more poorly at reproducing the macroscopic and single-channel results than the one with absolutely coupled subunits because it allows more closed-state inactivation.

Since simple independent subunit models are inadequate to explain the data, we are faced with generating more elaborate schemes for each subunit or considering interactions between the subunits. Other more complex independent subunit schemes, such as ones in which each subunit possesses two C states, an O state, and an I state, may be generated which produce voltage-independent open times and burst parameters. However, we believe that many of these models will suffer from having too much closed-state inactivation, a problem that can be alleviated by partially coupled models.

Partially coupled model. The previously mentioned problems with the independent activation and inactivation model and the independent subunit models have led us to make the following modifications: (*a*) Inactivation is allowed only from closed states near to the open state. (*b*) The last opening step is fast and not voltage dependent. This is essential to reproduce the lack of voltage dependence of the open durations, the burst closed durations, and the number of openings per burst, which it does by allowing the last closed state to act as a buffer that insulates the open state from the voltage-dependent closing rate β.

These modifications give rise to the following scheme:

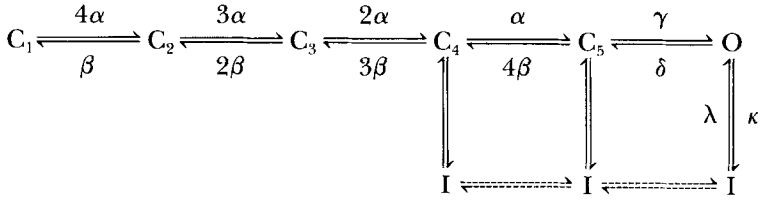

(Scheme 8)

where γ, δ, κ, and λ are independent of voltage. Inactivation can come from either C_4 or from both C_4 and C_5 but not only from C_5. Inactivation from only C_5 would give no voltage dependence to closed-state inactivation because there is no voltage-dependent pathway from the inactivatable state to the open state. Transitions between the inactivated states (*dashed arrows*) are possible, although our data do not address their presence. These transitions would allow the channel to recover from inactivation without opening.

We have tested this model, as before, by simultaneously fitting the single-channel and macroscopic data. Fig. 12 shows fits of scheme 8 to the open-duration distribution, first-latency distribution, number of openings per burst frequency histogram, and burst closed-duration distribution from a cell-attached patch containing a single A_1 channel, with voltage steps to 0 mV. Fig. 13 shows similar fits to data from the same patch obtained with steps to +50 mV. As can be seen, the model adequately reproduces these single-channel distributions and their voltage dependence. Satisfactory fits were obtained with similar values of the rate constants for the distributions of five other single-channel patches over a voltage range of −20 to +50 mV.

Scheme 8 also reproduces the macroscopic properties of the channels. Fig. 14, *A* and *B* show the ensemble averages for voltage steps to 0 and +50 mV from the same patch as shown in Figs. 12 and 13. Superimposed on these averages is the prediction of the partially coupled model for steps to these voltages. Because the single-channel current-voltage relation is linear over the voltage range −20 to +80 mV (Zagotta et al., 1988), macroscopic currents [$I(t)$] can be calculated from the channel open probabilities [$P(t)$] and membrane potential (V) using the following equation:

$$I(t) = Ng(V - E_r)P(t) \quad (6)$$

where the single-channel conductance (g) is 15 pS, the reversal potential (E_r) is −54 mV (Zagotta et al., 1988), and the number of channels (N) is constant for any given

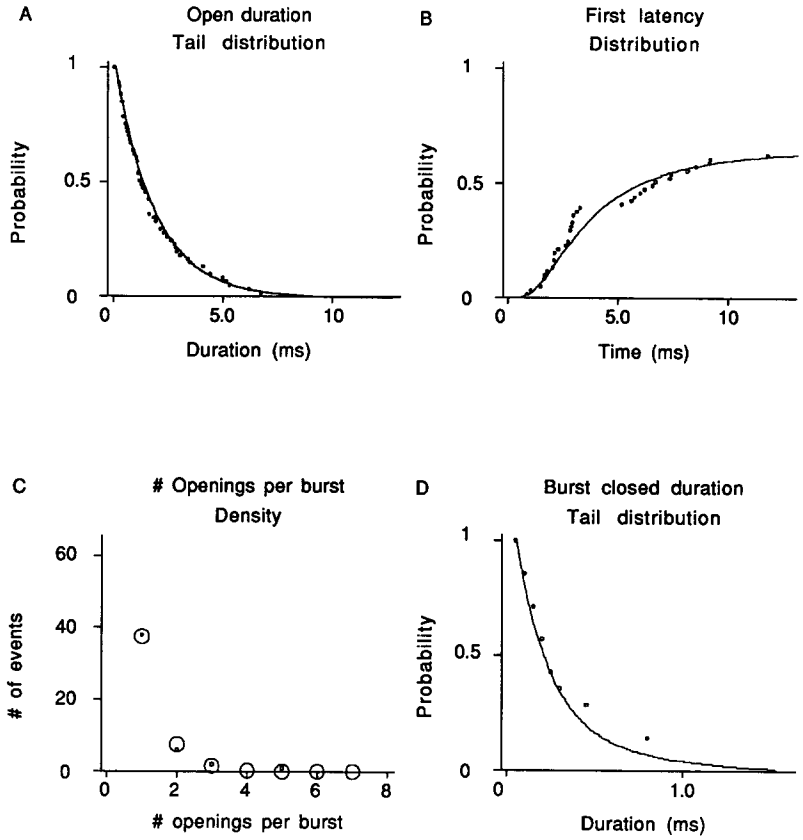

FIGURE 12. Fits of scheme 8 to the single-channel parameters from a cell-attached patch during voltage steps to 0 mV. (*A*) Tail distribution of open durations is shown as dots and fitted by the prediction of the model, a single-exponential distribution with a time constant of 2.0 ms. (*B*) Distribution of first latencies shown as dots fitted by the first-latency distribution calculated numerically from the model. (*C*) Frequency histogram of the number of openings per burst is shown as dots and fitted by the prediction of the model, a geometric distribution (Eq. 2) with the probability of terminating the burst (q) equal to 0.8, shown as circles around the dots. The criterion for burst termination was a closure of more than 1 ms. (*D*) Tail distribution of the burst closed durations shown as dots and fitted by the burst closed duration tail distribution calculated numerically from the model. The shortest bin (50 μs) was not considered in the fits and is not plotted on the graph.

cell. Fig. 14 *C* shows macroscopic A currents for a family of voltage steps between -30 and $+50$ mV calculated from scheme 8 with Eq. 6. These calculated currents are compared in Fig. 14 *D* with experimental whole-cell records from a cell that had little noninactivating current. These currents exhibit voltage dependence and kinetics that are very similar to the calculated currents.

Fig. 15 *A* shows resting inactivation curves from seven different myotubes fitted with the equilibrium solution (Eq. 4) to scheme 8. Although the state diagram is

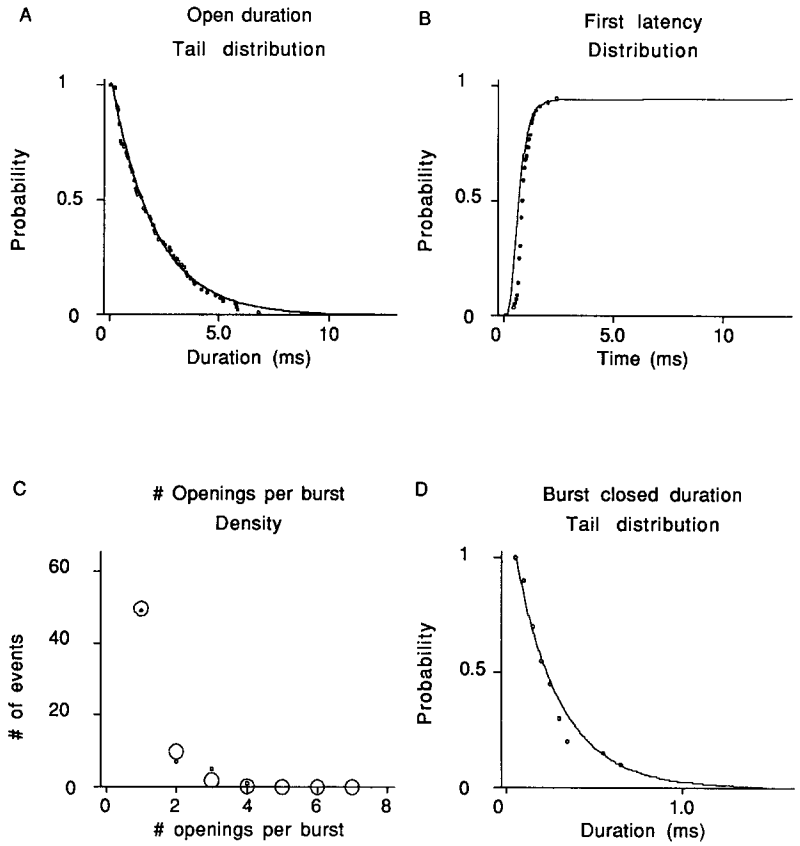

FIGURE 13. Fits of scheme 8 to the single-channel parameters from a cell-attached patch during voltage steps to +50 mV. (*A*) Tail distribution of open durations is shown as dots and fitted by the prediction of the model, a single-exponential distribution with a time constant of 2.0 ms. (*B*) Distribution of first latencies shown as dots fitted by the first latency distribution calculated numerically from the model. (*C*) Frequency histogram of the number of openings per burst is shown as dots and fitted by the prediction of the model, a geometric distribution (Eq. 2) with the probability of terminating the burst (q) equal to 0.8, shown as circles around the dots. The criterion for burst termination was a closure of more than 1 ms. (*D*) Tail distribution of the burst closed durations shown as dots and fitted by the burst closed duration tail distribution calculated numerically from the model. The shortest bin (50 μs) was not considered in the fits and is not plotted on the graph.

much more complicated than a two-state model for inactivation, the fit is essentially indistinguishable from a Boltzmann distribution (Eq. 1) with a midpoint ($V_{1/2}$) of −29 mV and a slope factor (Y) of 3.5 mV corresponding to an equivalent gating charge of seven electronic charges. This gating charge comes entirely from transitions between closed states as no other transitions are voltage dependent. The value for the equivalent charge derived from the Boltzmann distribution is less than the total amount of charge (9.4 electronic charges, see below) that actually moves in the

model between the left-most closed state and the open state. This was a general feature of all of the partially coupled models we tested.

Resting inactivation was important in the fitting process as it contributed substantially to the determination of β, which is low at depolarized voltages where the single-channel duration distributions were measured. Because of the high dependence of β values on the resting inactivation curve, these values are sensitive to possible differences in voltage dependence between the cell-attached and outside-out configurations, where the single-channel activity was recorded, and the whole-cell configuration, where the resting inactivation was recorded. Although it is unlikely that changes in membrane potential between the two configurations were large, differences in voltage dependence of gating between patches and whole cells have been

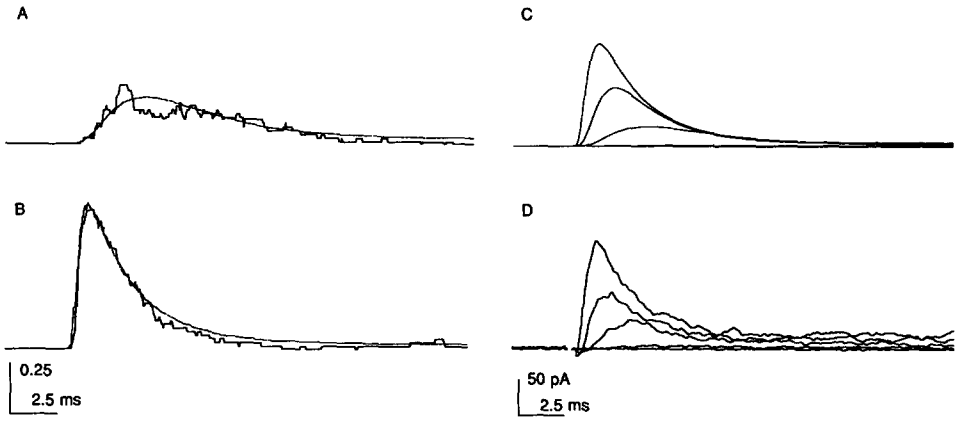

FIGURE 14. Fits of scheme 8 to ensemble averages and macroscopic currents. (*A*) Ensemble average from a single-channel cell-attached patch during voltage steps to 0 mV plotted as probability. Superimposed on the data is the open probability after a voltage step to 0 mV calculated numerically from the model. (*B*) Ensemble average from the same patch as (*A*) during voltage steps to +50 mV superimposed on the open probability calculated numerically from the model. (*C*) Family of macroscopic currents calculated numerically from the model using Eq. 6 for voltage steps to −30, −10, +10, +30, and +50 mV. (*D*) Family of whole-cell currents recorded during voltage steps to the same voltages as *C*. This myotube contained an unusually small delayed-rectifying potassium current and therefore its kinetics are minimally contaminated by poor current separation.

reported for sodium channels (Fenwick et al., 1982; Marty and Neher, 1983; Fernandez et al., 1984). To the extent that the resting inactivation curve has shifted to more negative voltages, β will be smaller than we have calculated. A 10-mV shift between whole-cell and single-channel voltage dependence will decrease the amplitude of β by 60% with no effect on β's voltage dependence. The rest of the rate constants in the model will not be influenced.

Because the models can reproduce the open probabilities after voltage steps, the predictive power of scheme 8 was tested for other commonly measured voltage-dependent properties of macroscopic currents. Fig. 15 *B* shows a comparison of experimentally determined and calculated time-to-peak current vs. membrane

potential. The time-to-peak was measured directly from families of whole-cell currents for the data points and from currents numerically calculated from scheme 8 for the smooth curve. A comparison of the experimentally determined and calculated peak conductance-voltage relation [$G(V)$] is shown in Fig. 15 *C*. The experimental $G(V)$ was determined from a number of whole-cell current families by dividing the peak minus steady-state current by the single-channel current at the same

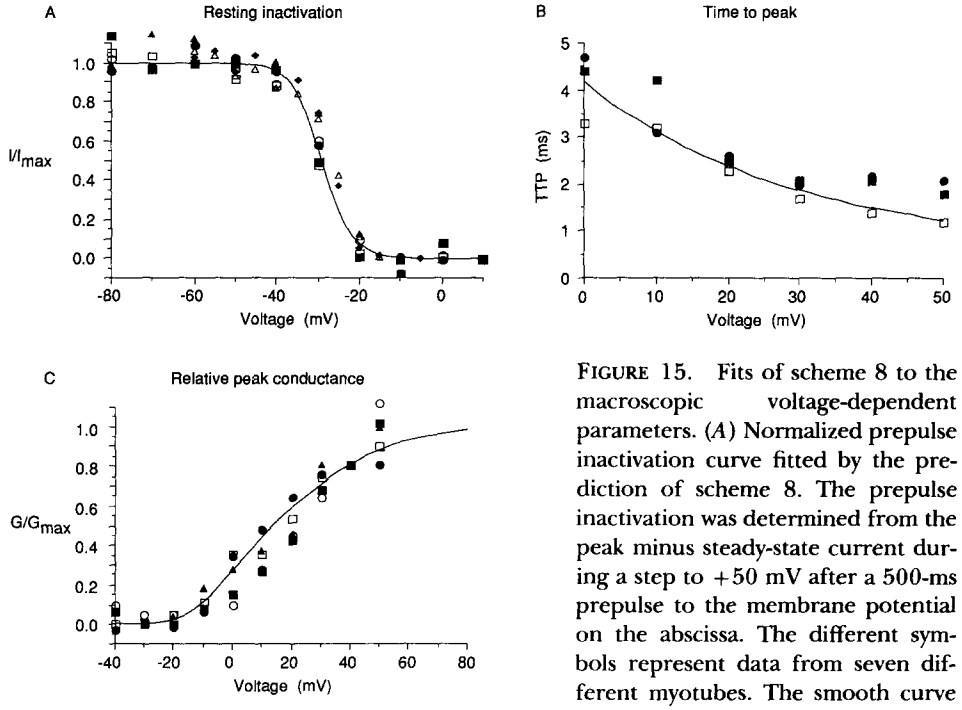

FIGURE 15. Fits of scheme 8 to the macroscopic voltage-dependent parameters. (*A*) Normalized prepulse inactivation curve fitted by the prediction of scheme 8. The prepulse inactivation was determined from the peak minus steady-state current during a step to +50 mV after a 500-ms prepulse to the membrane potential on the abscissa. The different symbols represent data from seven different myotubes. The smooth curve is the equilibrium probability of remaining activatable and was calculated from the model by Eq. 4. (*B*) Time-to-peak vs. step potential from myotube whole-cell currents fitted with the prediction of the model. The different symbols represent data from three different myotubes. The smooth curve was determined from the model by calculating numerically the probability of being open after voltage steps and measuring the time-to-peak from the calculated waveforms. (*C*) Normalized peak conductance vs. membrane potential curve $G(V)$ from myotube whole-cell currents fitted by the prediction of the model. Peak conductance was calculated from the peak minus steady-state whole-cell currents using Eq. 6. The different symbols represent data from five different patches. The smooth curve was determined from the model by measuring the peak from the calculated waveforms.

membrane potential and normalizing to 0.81 at +40 mV. For the $G(V)$ prediction of scheme 8, represented by the smooth curve, a similar calculation was performed on the calculated currents.

The values of the rate constants used in the fits are summarized in Fig. 16. The model diagrammed in Fig. 16 *A* shows the voltage-independent rate constants near the arrows corresponding to the relevant transitions. The voltage dependence of the activation rate constants (α and β) is plotted in Fig. 16 *B* and expressed as an equa-

tion in Fig. 16 *C*. The model with these rates fits the single-channel distributions from a single patch (Figs. 12, 13, and 14) and the macroscopic behavior of A currents in many whole-cell experiments (Figs. 14 and 15). The close agreement between the predicted and actual data indicates the adequacy of scheme 8 for the voltage-dependent gating of *Shaker* A channels. Although detailed fits of theoretical distributions are shown from a single patch, only minor changes were required for other patches, and the model accurately predicts the macroscopic behavior of a large population of channels in a number of cells.

Rate constants enclosed in boxes in Fig. 16 *A* are not dependent upon membrane potential and therefore do not involve movement of charged particles through the membrane field. From these rates, the free energy differences between the various states (ΔG) can be calculated with the following equation:

$$\Delta G = -RT \ln\left(\frac{k_1}{k_{-1}}\right) \tag{7}$$

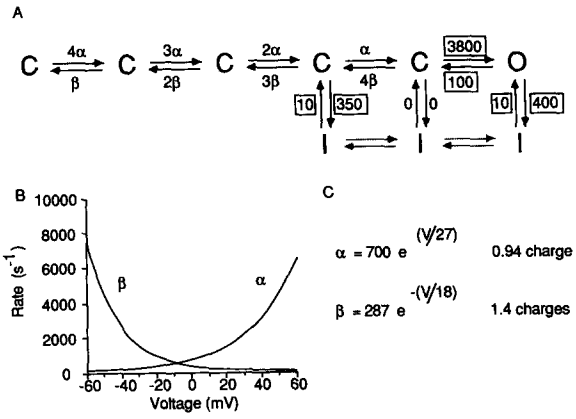

FIGURE 16. Summary of the rates used in scheme 8, which fit all of the macroscopic and single-channel parameters. (*A*) State diagram of the model showing the absolute magnitudes of the voltage-independent rates (s^{-1}) and the relative magnitudes of the voltage-dependent rates. The rate constants that do not depend on voltage are boxed. Since this channel exhibited little voltage-independnet closed-state inactivation, the inactivation rate from the right-most closed state was zero. Some channels exhibited more blank sweeps at +50 mV (see Fig. 9), suggesting a slow inactivation rate from the right-most closed state. (*B*) Exponential voltage dependence of the activation and deactivation rates (Eq. 3). (*C*) Equations for the activation and deactivation rates showing the equivalent charge movement associated with these rates.

where R is the universal gas constant, T is the absolute temperature, k_1 is the rate of the forward reaction, and k_{-1} is the rate of the reverse reaction. This free energy difference indicates the relative stability of the different channel conformations represented by different states. Table I shows the energy differences between all of the pairs of states at 0 mV. The 2 kcal/mol stabilization of the open state relative to the last closed state, and of the inactivated state relative to the open state is equivalent to approximately half the energy for the formation of a hydrogen bond.

In addition, the activation energy between each state and its neighbors ($\Delta G^{\ddagger}$) can be estimated with the following equation:

$$\Delta G^{\ddagger} = -RT \ln\left(\frac{k}{\upsilon}\right) \tag{8}$$

where k is the transition rate, and v is the product of the transmission coefficient and the molecular vibration frequency and is assumed here to have a value of 10^{12} s^{-1}. The calculated energy barriers for all of the transitions in the model lie between 12 and 15 kcal/mol. This is approximately five times the energy for rotation around carbon-carbon single bonds, and is significantly greater than the thermal energy (0.6 kcal/mol).

α and β are the only voltage-dependent rate constants. These rates represent the forward and backward rates for the individual activation assemblies or subunits. The equivalent charge movements between each closed state and the transition state to a neighboring closed state ($z^{\ddagger}$) can be calculated by the following equations:

$$z_{\alpha}^{\ddagger} = \frac{RT}{FV_{\alpha}} \quad \text{and} \quad z_{\beta}^{\ddagger} = \frac{RT}{FV_{\beta}} \tag{9}$$

This equivalent charge movement through the membrane is 0.94 electronic charges

TABLE I

Relative Free Energies of Pairs of States and Transition States in Scheme 8 at 0 mV

Transition	ΔG (kcal/mol)	$\Delta G^{\ddagger}$ (kcal/mol) forward	$\Delta G^{\ddagger}$ (kcal/mol) reverse
C ⇌ C*	−0.6	12.4	12.9
C ⇌ O	−2.1	11.4	13.5
O ⇌ I	−2.1	12.7	14.9
C ⇌ I	−2.2	12.8	14.9

Relative free energies of pairs of states and transition states in scheme 8 at 0 mV. The free energy differences between all of the pairs of states (ΔG) was calculated using Eq. 7. The free energy of activation between each state and the transition to neighboring states ($\Delta G^{\ddagger}$) was calculated using Eq. 8. The frequency factor (ν) was assumed to be 10^{12} s^{-1}. The energies for the C to C* transitions are those for the activation transition of each subunit at 0 mV. All other transition energies were voltage independent.

in the forward direction (α) and 1.4 electronic charges in the reverse direction (β). This corresponds to an equivalent charge movement of 2.3 electronic charges. Approximately 40% of the total charge movement for the transition occurs between the closed state of each subunit and the transition state to the activated conformation. In addition to the differences in charge distribution, the closed and activated states of the subunits differ in free energy by 0.6 kcal/mol at 0 mV, which is approximately equivalent to thermal energy.

DISCUSSION

We have analyzed the gating of single native A-type potassium channels that are coded for, at least in part, by the *Shaker* gene. The studies were carried out in cultured embryonic myotubes from *Drosophila,* where the standard artifacts associated with whole-cell recording, such as current separation and space-clamp, were potential problems. These problems were largely eliminated by confirmation of many of

the macroscopic experimental results with ensemble averages from single-channel patches.

We have arrived at the following general conclusions about A_1 channel gating that do not rely on any of our particular models or assumptions. (*a*) They possess a single, kinetically discernible open state. (*b*) After opening, the channel can enter a resting state or a longer lived inactivated state. (*c*) All transitions after first opening, including the inactivation transition itself, are not voltage dependent. (*d*) A resting channel must traverse at least two closed states before opening. (*e*) At least some of the transitions along the opening pathway are voltage dependent. (*f*) The voltage-dependent opening transitions account for the voltage dependence of macroscopic currents. (*g*) Inactivation of the channel is strongly coupled to activation. (*h*) The small amount of inactivation from closed states is more pronounced at lower voltages.

After trying a number of different kinetic models, we have concluded that some of the gating properties are likely to come about from aggregate properties of the subunits and cannot be accounted for by assuming the independent action of multiple subunits. Models in which activation is independent of inactivation, or where subunits, which both activate and inactivate, are independent of each other, were insufficient to explain all of the single-channel and macroscopic data. These independent models failed for the same basic reasons. Both contained a voltage-dependent transition entering and leaving the open state, which produces voltage-dependent open durations or number of openings per burst, and voltage-dependent burst closed durations, none of which shows measurable voltage dependence. In addition, both models predicted an unusually high occurrence of closed-state inactivation, especially at high voltages, where few blank records are actually observed. In order to overcome these deficiencies, the models were modified to contain a voltage-independent opening transition and closed-state inactivation only from a small number of closed states. Both of these modifications represent aggregate properties that cannot be explained in terms of an independent model.

A number of assumptions and constraints for candidate models were made to reduce the number of parameters that needed to be specified. While there is little evidence for or against these constraints, we believe they represent the simplest assumptions. The effect of relaxing some of these constraints would be to invalidate some of the quantitative conclusions obtained from the model. If the activation of each subunit is not independent, exhibiting some cooperativity for example, or identical, as would be the case if the channel was a heteromultimer of kinetically different subunits, the measurements of the activation rates and voltage dependence would be inaccurate. The assumption of an exponential dependence on membrane potential of the activation rates, which seems to hold at voltages greater than 0 mV, allowed us to make a simple estimate of the charge movement associated with these transitions. To the extent that this assumption no longer holds at voltages where the resting inactivation changes, our estimates of charge movement will be in error. If the channel were composed of more than four subunits, the voltage dependence, and hence the charge movement, associated with the activation transitions would be overestimated, or conversely, underestimated if the channel contained less than four subunits.

Not all of the rates specified in the model were equally well determined. All of the rates into and out of the open state, except the I → O rate λ were measured by fits to the single-channel histograms. The parameters for α ($A\alpha$ and $V\alpha$) were determined primarily from fits to the first latencies at different voltages, and those for β ($A\beta$ and $V\beta$) were determined from fits to the prepulse inactivation relation. All of the above rates are completely specified by the histograms and changes of 10% in any of them significantly impaired the fits. λ was inferred from the interburst closed durations and steady-state current in the ensemble average, two parameters which vary significantly from patch to patch. The closed-state inactivation rates were determined from the probabilities of blank records (Fig. 9), which also varies between different patches. These latter rates were therefore the least well determined and should be taken as only approximate.

The model predicts little voltage dependence of the tail current kinetics because of voltage independence of the rates leaving the open states, δ and κ. If the probability of terminating a burst (q in Fig. 6 *C*) is between 0.4 and 0.9, the primary time constant of the tails would be expected to decrease by 10–60% at voltages significantly below −20 mV. We have been unable to measure reliably tail currents because of the lack of sufficient current separation from the delayed currents (see Fig. 1). Our experiments only address the potential voltage dependence of δ and κ at voltages above −40 mV. A larger voltage dependence of tail currents below −40 mV would suggest a modification of the model such that δ becomes voltage dependent at more negative voltages. Spruce et al. (1989) have found only a small voltage dependence in tail kinetics between −50 and −90 mV for a delayed rectifier channel and have concluded that there is relatively little voltage dependence in the final opening step.

In addition to similarity in primary structure, the A_1 channel shares many similarities in voltage-dependent gating with the voltage-activated sodium channel. Analysis of the gating of single channels (Aldrich et al., 1983; Aldrich and Stevens, 1987; Barres et al., 1989; Kirsch and Brown, 1989) and gating currents (Armstrong and Bezanilla, 1977) from sodium channels has revealed that their inactivation is also nearly voltage independent and the voltage dependence of macroscopic sodium currents and resting inactivation comes about primarily from voltage-dependent activation transitions. This similarity in voltage-dependent gating is likely a reflection of the sequence similarity these proteins share in the S4 and neighboring regions. This region has been proposed to contain the voltage sensor for the channels, and perhaps contains much of the machinery needed to specify the mechanism described here. The similarity in both structure and function suggests a conserved mechanism for voltage-dependent gating between channels of different selectivities. The primary differences between the gating of A_1 channels and sodium channels are the higher probability of returning from inactivation and the lower probability of inactivating from closed states for the A_1 channel. These properties, and others as well, also differ between the native A channel and the A channels expressed by *Shaker* RNA in oocytes (Iverson et al., 1988; Timpe et al., 1988*a*, *b*; Zagotta et al., 1989) and may be influenced by sequences outside the regions of homology (especially near the amino and carboxyl terminals).

The charge movement determined in this study has implications for the proposed

S4 mechanism of voltage-dependent gating (Greenblatt et al., 1985; Catterall, 1986; Guy and Seetharamulu, 1986; Noda et al., 1986). In this mechanism a twisting and sliding of the S4 helix through the membrane in response to changes in membrane potential is responsible for the charge movement associated with activation. Every third amino acid of the S4 region is positively charged and thought to be paired with a negatively charged residue from the other transmembrane helices. According to this model the sliding of the helix is likely to occur in an integral multiple of the distance covered by three amino acids. This theory predicts an equivalent charge movement of approximately one electronic charge per three residue movement per subunit. The charge movement determined in the model per subunit is 2.3 electronic charges, suggesting either that the S4 moves at least two ratchets, or that there is considerable charge movement elsewhere in the protein that contributes to the voltage-dependent gating mechanism.

Many naturally occurring and induced variants of *Shaker* A channels have been found that alter its gating mechanism. One EMS-induced *Shaker* allele, *Sh5*, displays an altered kinetics and voltage dependence in its A current (Salkoff and Wyman, 1981*b*; Wu and Haugland, 1985; Zagotta, W. N., and R. W. Aldrich, manuscript in preparation). The different alternatively spliced variants have been shown to exhibit different macroscopic rates of inactivation and recovery from inactivation (Iverson et al., 1988; Timpe et al., 1988*a*, *b*; Zagotta et al., 1989). Site-directed mutants will provide a large number of additional variants. This model provides a framework in which to organize and understand the alterations in gating apparent in these channel variants.

We thank Drs. Denis Baylor, Toshinori Hoshi, and Thomas Schwarz for helpful comments on the manuscript.

This work was supported by U.S. Public Health Service grant NS-23294 to R. W. Aldrich and Training Grant NS-07158 to W. N. Zagotta.

Original version received 6 February 1989 and accepted version received 31 May 1989.

REFERENCES

Aldrich, R. W., D. P. Corey, and C. F. Stevens. 1983. A reinterpretation of mammalian sodium channel gating based on single-channel recording. *Nature.* 306:436–441.

Aldrich, R. W., and C. F. Stevens. 1987. Voltage-dependent gating of single sodium channels from mammalian neuroblastoma cells. *Journal of Neuroscience.* 7:418–431.

Armstrong, C. M. 1969. Inactivation of the potassium conductance and related phenomena caused by quaternary ammonium ion injection in squid axons. *Journal of General Physiology.* 54:533–575.

Armstrong, C. M., and F. Bezanilla. 1977. Inactivation of the sodium channel. II. Gating current experiments. *Journal of General Physiology.* 70:567–590.

Barres, B. A., L. L. Y. Chun, and D. P. Corey. 1989. Glial and neuronal forms of the voltage-dependent sodium channel: characteristics and cell-type distribution. *Neuron.* 2:1375–1388.

Baumann, A., I. Krah-Jentgens, R. Muller, F. Muller-Holtkamp, R. Seidel, N. Kecskemethy, J. Casal, A. Ferrus, and O. Pongs. 1987. Molecular organization of the maternal effect region of the *Shaker* complex of *Drosophila:* characterization of an I_A channel transcript with homology to vertebrate Na^+ channel. *European Molecular Biology Organization Journal.* 6:3419–3429.

Catterall, W. A. 1986. Voltage-dependent gating of sodium channels: correlating structure and function. *Trends in Neuroscience.* 9:7–10.

Connor, J. A., and C. F. Stevens. 1971. Voltage-clamp studies of a transient outward membrane current in gastropod neural somata. *Journal of Physiology.* 213:21–30.

Cooper, E., and A. Shrier. 1985. Single-channel analysis of fast transient potassium currents from rat nodose neurones. *Journal of Physiology.* 369:199–208.

Ellis, S. B., M. E. Williams, N. R. Ways, R. Brenner, A. H. Sharp, A. T. Leung, K. P. Campbell, E. McKenna, W. J. Koch, A. Hui, A. Schwartz, and M. M. Harpold. 1988. Sequence and expression of mRNAs encoding the α_1 and α_2 subunits of a DHP-sensitive calcium channel. *Nature.* 241:1661–1664.

Fenwick, E. M., A. Marty, and E. Neher. 1982. Sodium and calcium channels in bovine chromaffin cells. *Journal of Physiology.* 331:599–635.

Fernandez, J. M., A. P. Fox, and S. Krasne. 1984. Membrane patches and whole-cell membranes: a comparison of electrical properties in rat clonal pituitary (GH_3) cells. *Journal of Physiology.* 356:565–585.

French, R. J., and R. Horn. 1983. Sodium channel gating: models, mimics and modifiers. *Annual Review of Biophysics and Bioengineering.* 12:319–356.

Greenblatt, R. E., Y. Blatt, and M. Montal. 1985. The structure of the voltage-sensitive sodium channel. Inferences derived from computer-aided analysis of the *Electrophorus electricus* channel primary structure. *Federation of Experimental Biology Society Letters.* 193:125–134.

Guy, H. R., and P. Seetharamulu. 1986. Molecular model of the action potential sodium channel. *Proceedings of the National Academy of Sciences.* 83:508–512.

Hamill, O. P., A. Marty, E. Neher, B. Sakmann, and F. J. Sigworth. 1981. Improved patch clamp techniques for high-resolution current recording from cells and cell-free membrane patches. *Pflügers Archiv.* 391:85–100.

Hodgkin, A. L., and A. F. Huxley. 1952. A quantitative description of membrane current and its application to conduction and excitation in nerve. *Journal of Physiology.* 117:500–544.

Iverson, L. E., M. A. Tanouye, H. A. Lester, N. Davidson, and B. Rudy. 1988. A-type potassium channels expressed from *Shaker* locus cDNA. *Proceedings of the National Academy of Sciences.* 85:5723–5727.

Jan, Y. N., L. Y. Jan, and M. J. Dennis. 1977. Two mutations of synaptic transmission in *Drosophila. Proceedings of the Royal Society of London B.* 198:87–108.

Kamb, A., L. E. Iverson, and M. A. Tanouye. 1987. Molecular characterization of *Shaker,* a *Drosophila* gene that encodes a potassium channel. *Cell.* 50:405–413.

Kamb, A., J. Tseng-Crank, and M. A. Tanouye. 1988. Multiple products of the *Drosophila Shaker* gene may contribute to potassium channel diversity. *Neuron.* 1:421–430.

Kasai, H., M. Kameyama, K. Yamaguchi, and J. Fukuda. 1986. Single transient K channels in mammalian sensory neurons. *Biophysical Journal.* 49:1243–1247.

Kayano, T., M. Noda, V. Flockerzi, H. Takahashi, and S. Numa. 1988. Primary structure of rat brain sodium channel III deduced from the cDNA sequence. *Federation of Experimental Biology Society Letters.* 228:187–194.

Kirsch, G. E., and A. M. Brown. 1989. Kinetic properties of single sodium channels in rat heart and rat brain. *Journal of General Physiology.* 93:85–99.

MacKinnon, R., P. H. Reinhart, and M. M. White. 1988. Charybdotoxin block of *Shaker* K^+ channel suggests that different types of K^+ channels share common structural features. *Neuron.* 1:997–1001.

Marty, A., and E. Neher. 1983. Tight-seal whole cell recording. *In* Single-Channel Recording, B. Sakmann and E. Neher, editors. Plenum Publishing Co., New York. 107–121.

Neher, E. 1971. Two fast transient current components during voltage clamp on snail neurons. *Journal of General Physiology.* 58:36–53.

Noda, M., T. Ikeda, T. Kayano, H. Suzuki, H. Takeshima, M. Kurasaki, H. Takahashi, and S. Numa. 1986. Existence of distinct sodium channel messenger RNAs in rat brain. *Nature.* 320:188–192.

Noda, M., S. Shimizu, T. Tanabe, T. Takai, T. Kayano, T. Ikeda, H. Takahashi, H. Nakayama, Y. Kanaoka, N. Minamino, K. Kangawa, H. Matsuo, M. A. Raftery, T. Hirose, S. Inayama, H. Hayashida, T. Miyata, and S. Numa. 1984. Primary structure of *Electrophorus electricus* sodium channel deduced from cDNA sequence. *Nature.* 312:121–127.

Papazian, D. M., T. L. Schwarz, B. L. Tempel, Y. N. Jan, and L. Y. Jan. 1987. Cloning of genomic and complementary DNA from *Shaker,* a putative potassium channel gene from *Drosophila. Science.* 237:749–753.

Pongs, O., N. Kecskemethy, R. Muller, I. Kreh-Jentgens, A. Baumann, H. H. Klitz, I. Canal, S. Llamazares, and A. Ferrus. 1988. *Shaker* encodes a family of putative potassium channel proteins in the nervous system of *Drosophila. European Molecular Biology Organization Journal.* 7:1087–1096.

Salkoff, L. B. 1983. Genetic and voltage-clamp analysis of a *Drosophila* potassium channel. *Cold Spring Harbor Symposium on Quantitative Biology.* 48:221–231.

Salkoff, L., A. Butler, A. Wei, N. Scavarda, K. Giffen, C. Ifune, R. Goodman, and G. Mandel. 1987. Genomic organization and deduced amino acid sequence of a putative sodium channel gene in *Drosophila. Science.* 237:744–749.

Salkoff, L. B., and R. Wyman. 1981*a*. Outward currents in developing *Drosophila* flight muscle. *Science.* 212:461–463.

Salkoff, L. B., and R. Wyman. 1981*b*. Genetic modification of potassium channels in *Drosophila Shaker* mutants. *Nature.* 293:228–230.

Schwarz, T. L., B. L. Tempel, D. M. Papazian, Y. N. Jan, and L. Y. Jan. 1988. Multiple potassium channel components are produced by alternative spicing at the *Shaker* locus of *Drosophila. Nature.* 331:137–142.

Seecof, R. L. 1979. Preparation of cell cultures from *Drosophila melanogaster* embryos. *Tissue Culture Association Manual.* 5:1019–1022.

Seecof, R. L., and J. J. Donady. 1972. Factors affecting *Drosophila* neuron and myocyte differentiation in vitro. *Mechanisms of Ageing and Development.* 1:165–174.

Solc, C. K., and R. W. Aldrich. 1988. Voltage-gated potassium channels in larval CNS neurons of *Drosophila. Journal of Neuroscience.* 8:2556–2570.

Solc, C. K., W. N. Zagotta, and R. W. Aldrich. 1987. Single-channel and genetic analyses reveal two distinct A-type potassium channels in *Drosophila. Science.* 236:1094–1098.

Spruce, A. E., N. B. Standen, and P. R. Stanfield. 1989. Rubidium ions and the gating of delayed rectifier potassium channels of frog skeletal muscle. *Journal of Physiology.* 411:597–610.

Stevens, C. F. 1978. Interactions between intrinsic membrane proteins and electric field. An approach to studying nerve excitability. *Biophysical Journal.* 22:295–306.

Tanabe, T., K. G. Beam, J. A. Powell, and S. Numa. 1988. Restoration of excitation-contraction coupling and slow calcium current in dysgenic muscle by dihydropyridine receptor complementary DNA. *Nature.* 336:134–139.

Tanabe, T., H. Takeshima, A. Mikami, V. Flockerzi, H. Takahashi, K. Kangawa, M. Kojima, H. Matsuo, T. Hirose, and S. Numa. 1987. Primary structure of the receptor for calcium channel blockers from skeletal muscle. *Nature.* 328:313–318.

Taylor, P. S. 1987. Selectivity and patch measurements of A-current channels in *Helix aspersa* neurones. *Journal of Physiology.* 388:437–447.

Tempel, B. L., D. M. Papazian, T. L. Schwarz, Y. N. Jan, and L. Y. Jan. 1987. Sequence of a probable potassium channel component encoded at *Shaker* locus of *Drosophila*. *Science*. 237:749–753.

Thompson, S. H. 1977. Three pharmacologically distinct potassium channels in molluscan neurones. *Journal of Physiology*. 265:465–488.

Timpe, L. C., and L. Y. Jan. 1987. Gene dosage and complementation analysis of the *Shaker* locus in *Drosophila*. *Journal of Neuroscience*. 7:1307–1317.

Timpe, L. C., Y. N. Jan, and L. Y. Jan. 1988*a*. Four cDNA clones from the *Shaker* locus of *Drosophila* induce kinetically distinct A-type potassium currents in *Xenopus* oocytes. *Neuron*. 1:659–667.

Timpe, L. C., T. L. Schwarz, B. L. Tempel, D. M. Papazian, Y. N. Jan, and L. Y. Jan. 1988*b*. Expression of functional potassium channels from *Shaker* cDNA in *Xenopus* oocytes. *Nature*. 331:143–145.

Wu, C.-F., B. Ganetzky, F. N. Haugland, and A. X. Liu. 1983. Potassium currents in *Drosophila:* different components affected by mutations of two genes. *Science*. 220:1076–1078.

Wu, C.-F., and F. N. Haugland. 1985. Voltage clamp analysis of membrane currents in larval muscle fibers of *Drosophila:* alteration of potassium currents in *Shaker* mutants. *Journal of Neuroscience*. 5:2626–2640.

Zagotta, W. N., M. S. Brainard, R. W. Aldrich. 1988. Single-channel analysis of four distinct classes of potassium channels in *Drosophila* muscle. *Journal of Neuroscience*. 8:4765–4779.

Zagotta, W. N., T. Hoshi, and R. W. Aldrich. 1989. Gating of single *Shaker* potassium channels in *Drosophila* muscle and in *Xenopus* oocytes injected with *Shaker* mRNA. *Proceedings of the National Academy of Sciences*. 86:7243–7247.